

Negative index and mode coupling in all-dielectric metamaterials at terahertz frequencies

Éric Akmansoy & Simon Marcellin

Institut d'Électronique Fondamentale, Univ. Paris-Sud, Université Paris-Saclay,
Orsay, F-91405 ; UMR8622, CNRS, Orsay, F 91405.

E-mail: eric.akmansoy@u-psud.fr

Abstract. We report on the role of the coupling of the modes of Mie resonances in all-dielectric metamaterials to ensure negative effective index at terahertz frequencies. We study this role according to the lattice period and according to the frequency overlapping of the modes of resonance. We show that negative effective refractive index requires sufficiently strong mode coupling and that for even more strong mode coupling, the first two modes of Mie resonances are degenerated; the effective refractive index is then undetermined. We also show that adjusting the mode coupling leads to near-zero effective index, or even null effective index. Further, we compare the mode coupling effect with hybridization in metamaterials.

1. Introduction

All-dielectric metamaterials (ADM) are the promising “inflection” of metamaterials to go beyond their limits. ADMs are an alternative to metallic metamaterials. The advantages of ADMs come from their low losses and their simple geometry: they do not suffer from ohmic losses and thus benefit from low energy dissipation. From the microwave, their quality factor is greater than that of metallic metamaterials [1] and it is consequently at terahertz and optical frequencies. ADMs are partly inspired by the work of Richtmyer who developed the theory of dielectric resonators, which is based on the fact that “the dielectric has the effect of causing the electromagnetic field [...] to be confined to the cylinder itself and the immediately surrounding region of space.” [2]. Taking the matter further, O’Brien and Pendry opened the way for ADMs by considering the periodic lattice of high permittivity resonators (HPR), thus evidencing artificial magnetism in the microwave [3]. ADMs rely on the first two modes of Mie resonances of HPR. The first mode results in resonant effective permeability which can have negative values, while the second one results in resonant effective permittivity which can also have negative values. When the two are simultaneously negative, the ADM is called “double negative” (DNG) and its effective refractive index is then negative [4–9]. The unit cell of ADM thus comprises two subwavelength building blocks of simple geometry [10, 11]. By analogy with chemical molecules, the unit cell is generally called *meta-dimer* [12],

and the two building blocks are called *meta-atoms*. As the two are different, the unit cell is a hetero-dimer.

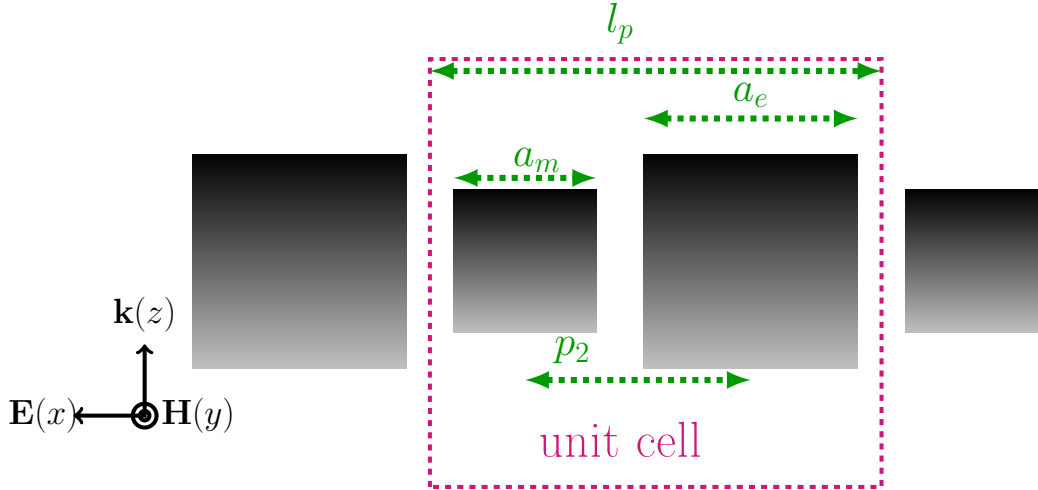


Figure 1. Schematic layout of the ADM. The ADM consists of one infinite layer along the x direction, and is made up of two interleaved sets of high permittivity square cross-section dielectric cylinders which resonate in the first two modes of Mie resonances: the small set resonates in the *magnetic* mode and the second one in the *electric* mode. The equidistant cylinders are infinite along the y direction and their side lengths are $a_m = 60 \mu m$ and $a_e = 90 \mu m$, respectively. Their relative permittivity is $\epsilon_r = 94$. The unit cell actually consists of two subwavelength distinct building blocks. The lattice period is $l_p = 260 \mu m$ and p_2 is half the lattice period. The incident wave is transverse electric (TE).

The large applications of ADMs (for a review, see ref. [13]) include perfect reflectors [14], perfect absorbers [15,16], zero-index metamaterials [17], optical magnetic mirror [18], Fano resonances [19,20]. ADMs have been demonstrated from microwave to optical domain. Artificial magnetism [1, 21–23] and negative effective refractive index [24,25] have been, theoretically and experimentally, evidenced in GHz range. Even though artificial magnetism provided by ADMs has been experimentally demonstrated in the THz range [26] and in the infrared range [27–30], DNG refractive index has not been yet demonstrated, which impede ADMs to be the equivalent of their metallic counterpart. Besides, terahertz (THz) radiation is widely defined as electromagnetic radiation in the frequency range 0.3-3 THz. Since it permits to obtain physical data which are not accessible using X-ray or infrared radiation, it finds many applications in imaging, security, quality inspection, chemical sensing, astronomy, etc. On their part, metamaterials have evolved towards the implementation of photonic components [31]. HPRs are well suited for metamaterials applications in the low THz frequency range [32].

In the following, we report on the mode coupling effect which plays a dominant role in the electromagnetic properties of metamaterials [33–36], notably, in the achievement of negative effective index. Magnetic and electric mode coupling effects in ADMs have

been separately studied from each other in the microwave by Zhang *et al* [34]. Herein, we report on the magneto-electric mode coupling effects going up the terahertz domain, and we show that negative effective refractive index requires sufficiently strong mode coupling [37]. We also show that adjusting the mode coupling allows to attain near-zero values of the refractive index, or even null effective index. Moreover, we highlight that the strongest values of the mode coupling lead to frequency mode degeneracy, for which the refractive index is undetermined.

2. Simulations

We considered a 2D ADM whose unit cell consists of two distinct building blocks, a *magnetic* block and an *electric* one, the former resonating in the first mode of Mie resonances and the latter resonating in the second mode [1, 11, 25, 38]. The first mode is thus referred to as the *magnetic* mode and the second one to as the *electric* mode. The ADM consists of one infinite layer made up of two sets of high permittivity square cross-section dielectric cylinders which are perpendicular to the incident wave vector (Fig.1). The two sets of HPRs are actually interleaved. The incident polarization is Transverse Electric (TE), i.e., the electric field is perpendicular to the axis of the cylinders. We studied both *spatial* mode coupling and *frequency* mode coupling. The ADM has been numerically simulated by the means of the finite elements method software HFSSTM which yields the *S*-parameters. The side lengths of the resonators are initially $a_m = 60 \mu m$ for the *magnetic* mode and $a_e = 90 \mu m$ for the *electric* one, the lattice period being $l_p = 260 \mu m$. The HPRs are equidistant and therefore, the distance between two of them is half the lattice period $p_2 = l_p/2 = 130 \mu m$. The relative permittivity of the dielectric is $\epsilon_r = 94$ (Titanium dioxide - TiO₂) and the loss tangent increases between $\tan \delta = 0.009$ and 0.015 in the considered frequency range [39, 40]. Thus, we are dealing with a high refractive index bulk material ($N_{TiO_2} \simeq 10$)

3. Results and discussion

3.1. Negative index and mode coupling

We studied the mode coupling between the first two modes of Mie resonances depending on the lattice period l_p (*spatial* mode coupling), and then depending on the frequency overlapping of the two modes (*frequency* mode coupling). The results of the simulation, namely the minimum $n_{eff_{min}}$ of the effective index n_{eff} in function the lattice period and in function of the frequency spacing between the two modes, are reported in Fig. 2 and 3, respectively. They show that the mode coupling should be strong enough to ensure negative effective index. The minima of the effective index n_{eff} are $n_{eff_{min}} = -2.2$ and -1.9 , respectively. In the one hand, increasing the mode coupling is obtained by decreasing the lattice period l_p . On the other hand, it is obtained by decreasing the frequency of the second mode of Mie resonances, which derives from the increasing of the side length a_e of the *electric* resonator. When the mode coupling is sufficient, the

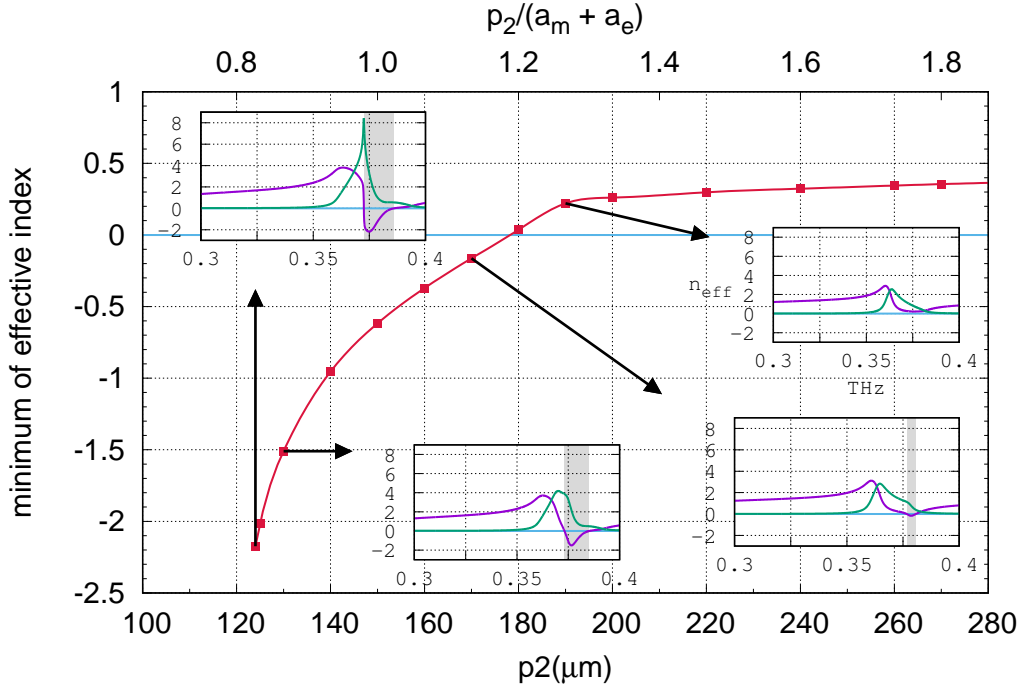


Figure 2. *Spatial mode coupling:* minimal value of the effective refractive index n_{eff} in function of the distance p_2 between two resonators. The side lengths of the resonators are $a_m = 60 \mu m$ and $a_e = 90 \mu m$, respectively. Insert: real and imaginary part of the effective index n_{eff} ; the shaded area denotes the bandwidth of negative effective index.

bandwidth of the negative effective index n_{eff} increases with it (see insets in Fig. 2 & 3). The frequency range of negative effective index is given by the relation [41]

$$\epsilon'(\omega) \cdot \mu''(\omega) + \epsilon''(\omega) \cdot \mu'(\omega) \leq 0, \quad (1)$$

where ' and '' respectively denote the real and imaginary parts of the permeability μ and the permittivity ϵ .

3.2. Monomode coupling

To carry out our study, we firstly studied monomode coupling, that is, the mode coupling due to only one mode, which arises inside a layer whose unit cell only consists of one building block, the *magnetic* one or the *electric* one. We studied both cases. Consequently, we had to only consider the *spatial* mode coupling and we only varied the lattice period l_p which is equal to the distance p_1 between two resonators, $l_p = p_1$. Operating in the same frequency range, the side length of the *magnetic* resonator is $a_m = 60 \mu m$, while that of the *electric* resonator is $a_e = 90 \mu m$. The results of the simulation are reported in Fig. 4 and 5, for both cases, and they show that the two modes differently behave. Their respective frequencies (f_{mr} , f_{er}) are given by the minima of

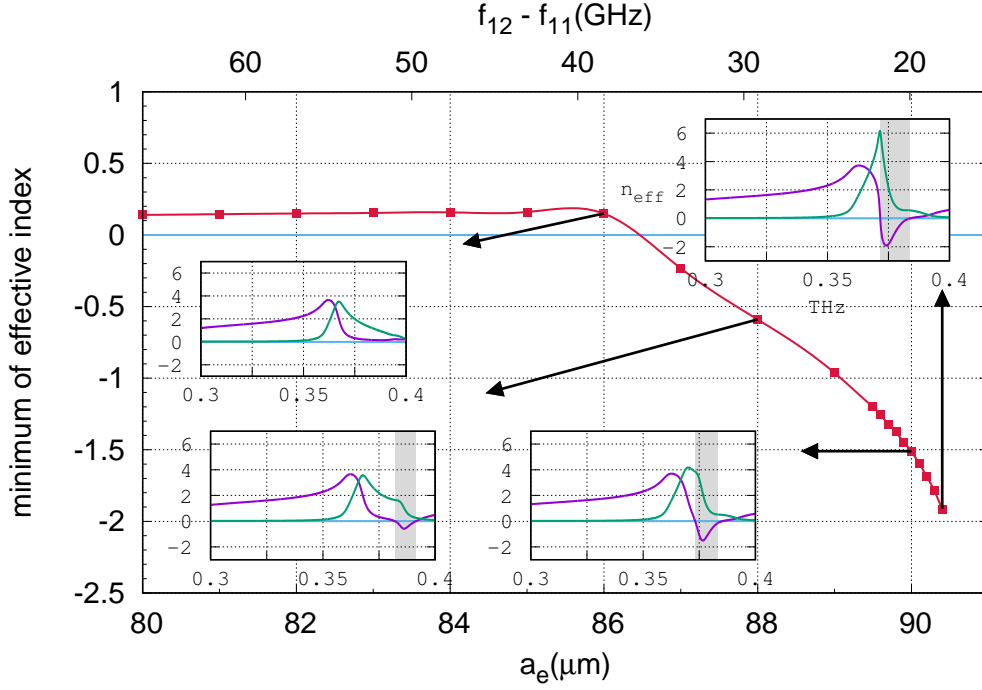


Figure 3. Frequency mode coupling: minimal value of the effective refractive index n_{eff} in function of the side length a_e of the *electric* resonator, namely, the frequency of the *electric* mode is varying. Insert: real and imaginary part of the effective index n_{eff} ; the shaded area denotes the bandwidth of negative effective index. f_{11} and f_{12} are the resonances frequencies of the individual resonators (see the text).

the S_{12} parameter [34]. The frequency f_{mr} of the *magnetic* mode increases with the lattice period l_p , whereas the frequency f_{er} of the *electric* one decreases. These results are consistent with that of reference [34]. Both maxima of the absorption A_{mr} and A_{er} ($A = 1 - |S_{12}|^2 - |S_{11}|^2$) and the frequency of the resonance modes of the individual resonator are also reported. This latter provides a series of resonances whose frequency is determined by Cohn's model [42–44]

$$f_{mn} = \frac{c}{2\sqrt{\epsilon_r}} \sqrt{\left(\frac{m}{a}\right)^2 + \left(\frac{n}{b}\right)^2}, \quad (2)$$

where ϵ_r is the relative permittivity of the resonator, m and n are integers, a and b are the side lengths of the resonator and c is the velocity of light and its accuracy is about 5%. Equation 2 was used to design all the reported structures. For square cross section cylinder, $a = b$, and the frequencies of the first two modes of the individual resonator respectively correspond to $m = n = 1$ and $m = 1$ and $n = 2$. To exhibit negative refractive index, the involved resonance modes are the first mode of the *magnetic* resonator and the second mode of the *electric* resonator. Their frequencies are respectively $f_{11} = 0.364$ THz ($a = a_m = 60 \mu m$) and $f_{12} = 0.384$ THz ($a = a_e = 90 \mu m$) [25]. These are obviously constant, while the maxima of the absorption

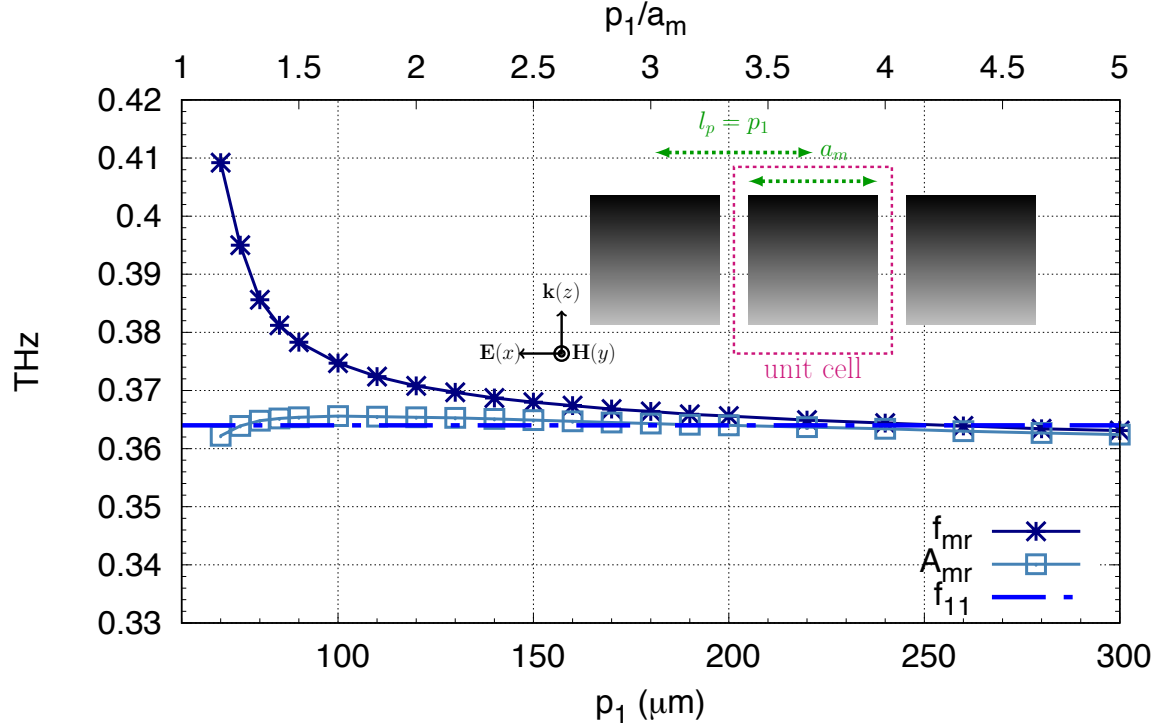


Figure 4. *Magnetic* mode coupling: frequency (f_{mr}) of the first mode of Mie resonances and of the maximum of absorption (A_{mr}) in function of the distance p_1 between two resonators. The unit cell only comprises the *magnetic* block. The side length of the resonator is $a_m = 60 \mu\text{m}$. The dashed line denotes the frequency of resonance (f_{11}) of the mode of resonances of the individual resonator.

are practically constant. It can be noticed that, as the mode coupling increases, the distance between the resonance frequencies (f_{mr} , f_{er}) of the resonator inside the layer and that (f_{11} , f_{12}) of the individual resonator respectively increases (cf. Fig. 4 and 5, respectively), thus evidencing the mode coupling.

3.3. Bimode coupling

Then, we studied the mode coupling inside the ADM, namely, the unit cell now consists of the two building blocks. The variation of the resonance frequencies (f_{mr} , f_{er}) of both modes is reported in Fig. 6 and 7 corresponding to the *spatial* mode coupling and the *frequency* mode coupling, respectively. These frequencies are still given by the minima of the S_{12} parameter [34]. Decreasing the lattice period l_p , i.e., the distance p_2 between the resonators, increases the mode coupling. Varying the overlapping of

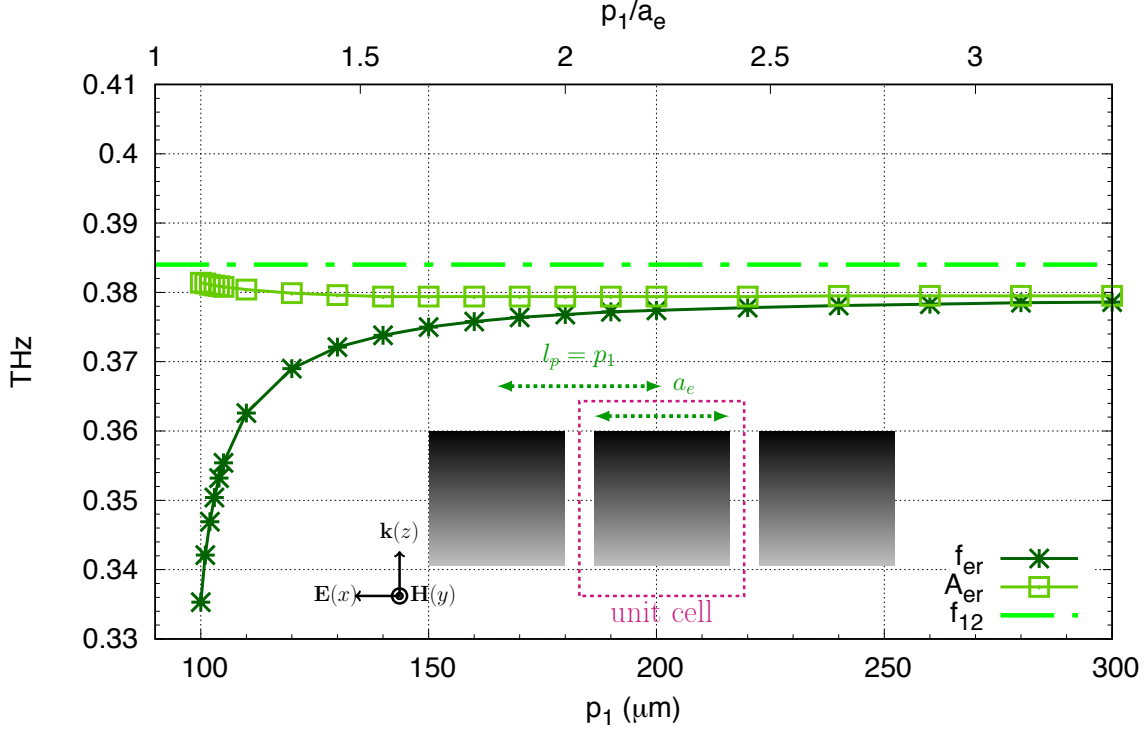


Figure 5. *Electric* mode coupling: frequency (f_{er}) of the second mode of Mie resonances and of the maximum of absorption (A_{er}) in function of the distance p_1 between two resonators. The unit cell only comprises the *electric* block. The side length of the resonator is $a_e = 90 \mu\text{m}$. The dashed line denotes the frequency of resonance (f_{12}) of the mode of resonances of the individual resonator.

the two modes stems from the decreasing of the frequency of the *electric* mode, which also increases the mode coupling [33]. The curves are shaped as “tuning forks” and show that the frequencies (f_{mr} , f_{er}) of the two modes of resonance are moving closer as the mode coupling increases. To highlight this effect, the frequencies (f_{11} , f_{12}) of the resonance modes of the individual resonator are again shown in these figures. For both the *magnetic* mode and the *electric* one, the distance between the frequency (f_{mr} , f_{er}) of the resonator inside the ADM and the frequency (f_{11} , f_{12}) of the individual one respectively increases as the mode coupling increases. This anew evidences the mode coupling inside the ADM. Theses curves also evidence that further increasing the mode coupling gives rise to a frequency degeneracy in both cases of mode coupling, that is, the two resonance frequencies of the two modes become equal, $f_{mr} = f_{er}$.

The S_{12} parameter and the absorption A are reported in Fig. 8 in function of the

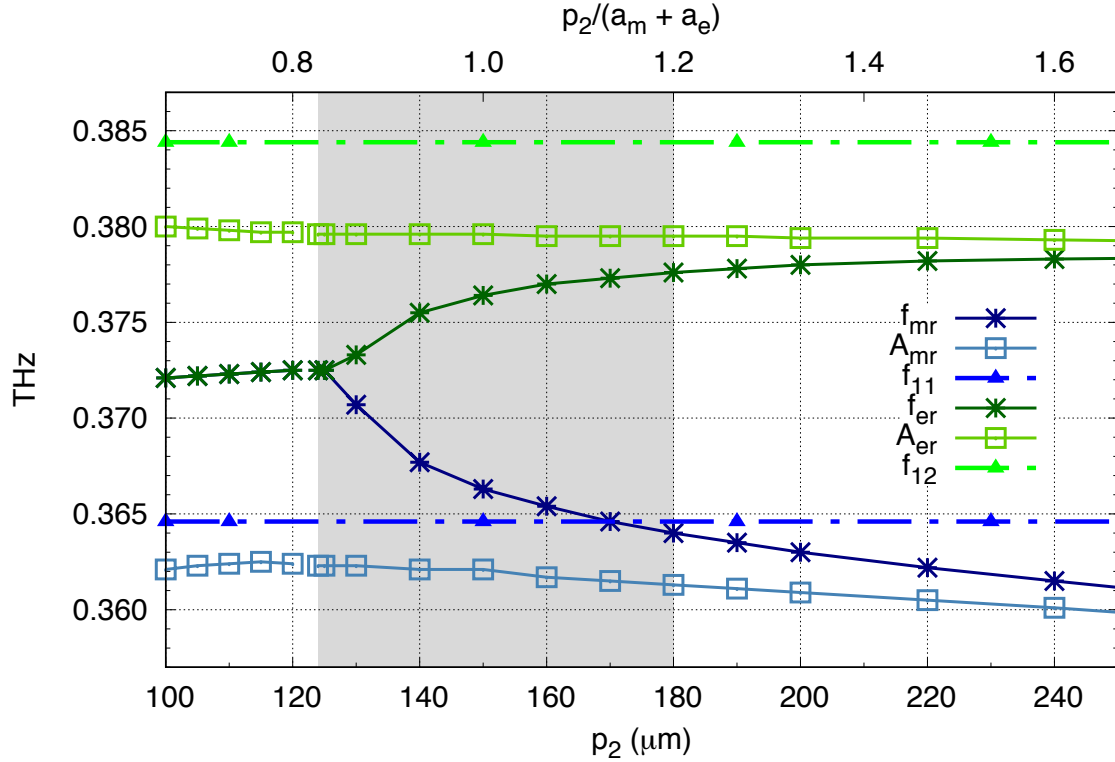


Figure 6. *Spatial* mode coupling: frequency of the first two modes of Mie resonances in function of the distance p_2 between two resonators which is half the lattice period l_p . Blue and green colors denote the *magnetic* and the *electric* modes, respectively. Square dots and crossed dots denote the maxima of absorption (A_{mr} , A_{er}) and the minimum of the S_{12} parameter (f_{mr} , f_{er}), respectively. The shaded area corresponds to negative value of the effective index n_{eff} . The side lengths of both resonators are $a_m = 60 \mu m$ et $a_e = 90 \mu m$, respectively. The dashed lines denote the frequencies of resonances (f_{11} , f_{12}) of the modes of the individual resonator.

frequency for several values of the lattice period l_p , which is relative to the *spatial* mode coupling. Two ranges of the lattice period l_p are considered, one is out of the frequency degeneracy regime ($250 \leq l_p \leq 400 \mu m$) and the second one in the frequency degeneracy regime ($200 \leq l_p \leq 248 \mu m$). It can be noticed that the frequency of both maxima of the absorption are practically constant, whereas the frequency of both minima of the S_{12} parameter are varying according to the lattice period l_p . These latter get closer as the lattice period l_p increases, until to be merged, which corresponds to the frequency degeneracy. The crossing point is reached when the lattice period is equal to $l_{pc} = 250 \mu m$. The merged minima of the S_{12} parameter attain very weak value ($\lesssim -51$ dB) for $l_p = 248 \mu m$, which corresponds to the minimum of the effective index $n_{eff_{min}}(l_p = 248 \mu m) = -2.2$. (See effective index curves inserted in Fig. 2 and Fig. 3 which are continuous, but are on the limit of continuity.) For greater values of the mode

coupling, that is, for lattice period l_p smaller than $248 \mu m$, the effective parameters could not be extracted, being not continuous through all frequencies [45]; the effective refractive index n_{eff} is then undetermined. We observed the same frequency degeneracy behavior when studying the *frequency* mode coupling (results not shown).

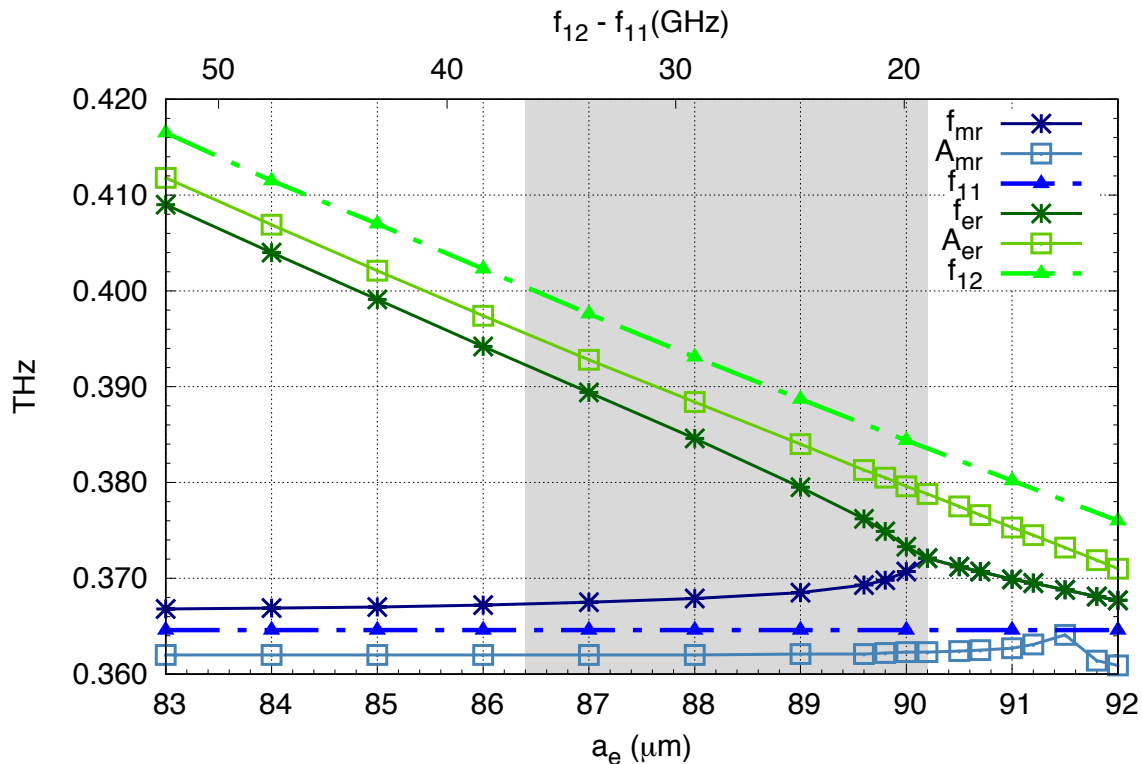


Figure 7. Frequency mode coupling: frequency of the first two modes of Mie resonances (f_{mr} , f_{er}) in function of the side length a_e of the *electric* resonator, namely, the frequency of the *electric* mode is varying. The convention is the same as in Fig. 6. The side length of the *magnetic* resonator is $a_m = 60 \mu m$ and the lattice period l_p is $260 \mu m$

The mode coupling effect we report on is different from hybridization [46] which is observed with plasmonic metamaterial [12, 47], split-ring resonators metamaterials [48], inductor-capacitor resonators [49], cut wires [50], nanowires [51], nano-rings [52], nanoparticle dimers [53] or silicon nanoparticles [54]. In the latter cases, the coupling between the two identical meta-atoms which constitute the dimer leads from a trapped mode to the formation of new hybridized modes because it lifts the degeneracy of the mode of the individual meta-atoms. Hybridization may be used to yield negative refractive index [48, 49, 52]. The unit cell is then a homo-dimer and the negative effective index is achieved by playing with the mode coupling so as to overlap two hybridized modes which are of different kind: *magnetic* or *electric*. In the case we report on, the mechanism is

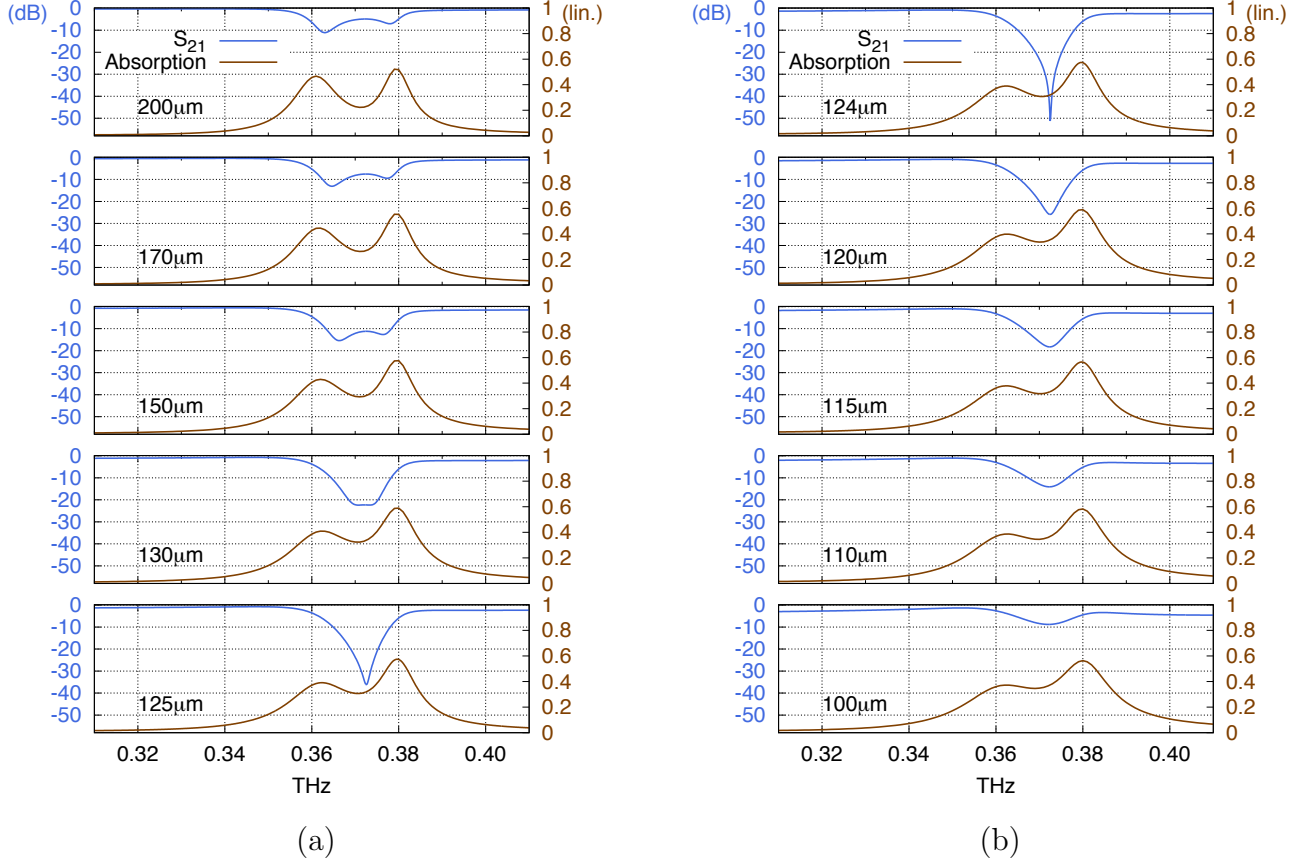


Figure 8. Effect of the *spatial* mode coupling: S_{12} parameter (log. scale (dB)) and absorption A (linear scale (lin.)) for several values of the distance p_2 between two resonators. The side lengths of the resonators are $a_m = 60 \mu m$ and $a_e = 90 \mu m$. (a) out of the frequency degeneracy regime ($125 \leq p_2 \leq 200 \mu m$); (b) in the frequency degeneracy regime ($100 \leq p_2 \leq 124 \mu m$). The merged minima of the S_{12} parameter attain very weak values ($\lesssim -51$ dB) when $p_2 = p_{2c} = 124 \mu m$, which correspond to the minimum of the refractive index $n_{eff_{min}} = -2.2$.

different since it takes the reverse way, because increasing the mode coupling leads from two separated modes to a trapped one. The unit cell of our ADM is a hetero-dimer because the two meta-atoms are not identical and moreover, each one resonates in a different kind of mode: the *magnetic* one and the *electric* one. Hence, increasing the mode coupling leads to the trapped mode putting together the two separated modes. Nevertheless, the mode coupling has to be strong enough to ensure negative effective index, the unit cell being either a homo-dimer or a hetero-dimer.

3.4. Effective parameters

In our ADM, a *magnetic* moment ensues from the *magnetic* mode giving rise to resonant effective permeability μ_{eff} . Similarly, an *electric* moment ensues from the *electric* mode giving rise to resonant effective permittivity ϵ_{eff} . The two of them are

perpendicular to each other (see e.g., Fig.1 in reference [38]). The mode coupling arises from the interaction between these electromagnetic moments and it changes with the distance between them. The side lengths of the resonators are afresh $a_m = 60 \mu m$ and $a_e = 90 \mu m$. Both resonances consequently modify the effective refractive index $n_{eff}(\omega)$ of the ADM. The effective electromagnetic parameters μ_{eff} , ϵ_{eff} and n_{eff} are reported in Fig.9 relative to two values of the lattice period $l_p = 360 \mu m$ and $l_p = 260 \mu m$. They are extracted from the S -parameters using the common retrieval method described in ref. [45, 55–60]. The antiresonance behavior of the effective permittivity ϵ_{eff} around the *magnetic* mode frequency, which is inherent in metamaterials, can be observed [60–63]. In the former case (low mode coupling), the effective index n_{eff} does not reach negative values, whereas it does in the latter case (strong mode coupling), then satisfying equation 1. The minimum value of the effective index is then $n_{eff_{min}}(l_p = 260 \mu m) = -1.5$. In the former case, the effective index n_{eff} is below unity and close to zero. Its minimal value is $n_{eff_{min}}(l_p = 360 \mu m) \lesssim 0.04$, evidencing that adjusting the mode coupling makes ADMs suitable for epsilon-near-zero (ENZ) metamaterials [64, 65] (see also Fig. 2), or even null effective index [17]. It can also be noticed that the mode coupling strongly enhances the amplitude of both resonances, notably the *electric* one, and that it brings closer the two modes. Besides, as we are dealing with a high refractive index bulk material ($N_{TiO_2} \simeq 10$), the wavelength inside it is about one-tenth of that in vacuum. Consequently, we calculated the static effective permittivity, i.e., beyond the resonances, from the Maxwell-Garnett model [66]. It is equal to $\epsilon_{eff} = 2.1$ and $\epsilon_{eff} = 2.9$ corresponding to both values of the lattice period $l_p = 360 \mu m$ and $l_p = 260 \mu m$, respectively, which is in good agreement with the results of the simulation.

To engineer the electromagnetic properties of an ADM, one can consequently play with either mode couplings: the *spatial* mode coupling or the *frequency* mode coupling. Fig.10 gather the role of both mode couplings: the stronger the two mode couplings, the more negative the effective index and the larger the bandwidth of negative effective index (cf. Fig. 2 and 3). Combining the two mode couplings, negative effective index as low as $n_{eff} = -2.8$ is obtained.

3.5. Dielectric function, phonons and strontium titanate (SrTiO₃)

Others high permittivity materials, having low losses, can be investigated to study the mode coupling inside ADMs at terahertz frequencies, e.g., SrTiO₃ [67–70]. However, the dielectric function $\epsilon_r(\omega)$ of these high permittivity materials is dispersive, because of the lattice vibrations, namely, the optical phonons [71]. Their frequency is in the THz range, and we are concerned by the transverse optical phonon of lowest frequency (TO₁). The TO₁ phonon frequency of SrTiO₃ is 2.70 THz [67], while that of TiO₂ is 5.6 THz [67, 71]. The dielectric function $\epsilon_r(\omega)$ is described by the classical oscillator model or the Four-Parameter Semi Quantum (FPSQ) model [67, 71]. Measurements at THz frequency, reported in the literature, are in good agreement with these models for

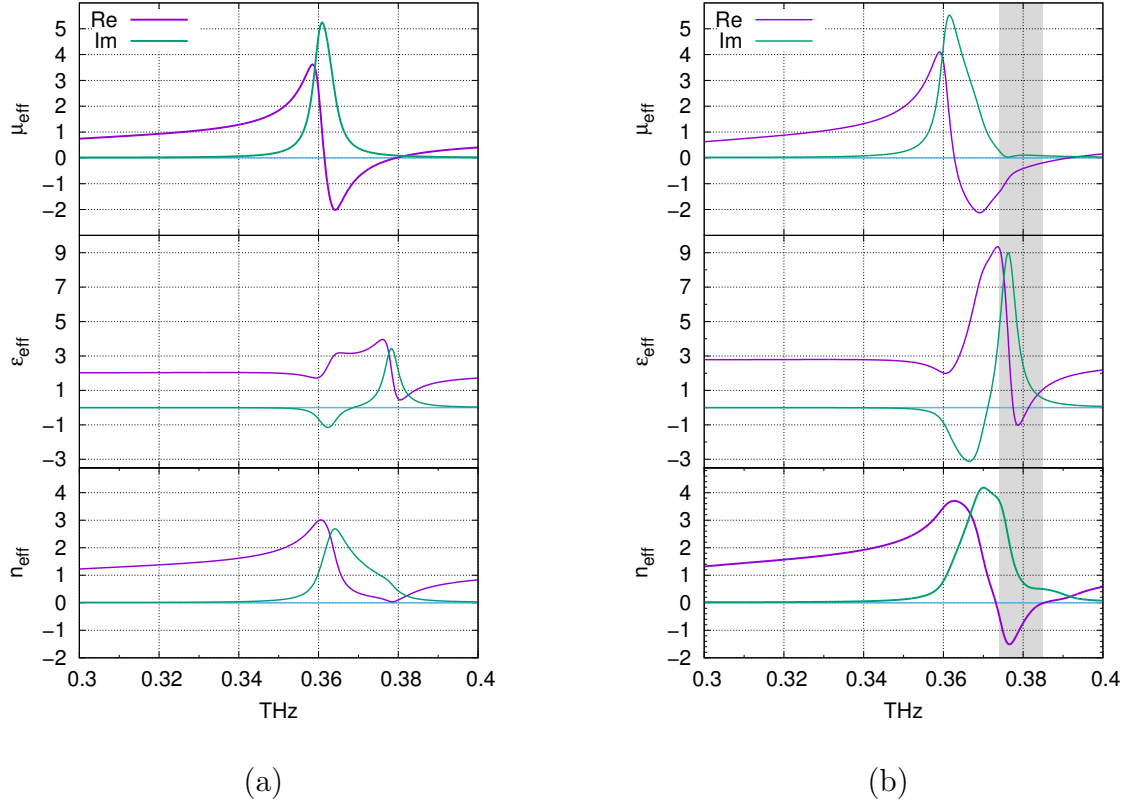


Figure 9. Effect of the *spatial* mode coupling: effective electromagnetic parameters (real and imaginary parts): permeability μ_{eff} (top), permittivity ϵ_{eff} (middle) and effective index n_{eff} (bottom). (a) low mode coupling: lattice period $l_p = 360 \mu\text{m}$: the minimum value of the effective refractive index is $n_{\text{eff}_{\text{min}}} \lesssim 0.04$; (b) strong mode coupling: lattice period $l_p = 260 \mu\text{m}$. The shaded area denotes the bandwidth of negative effective index: the minimum value of the effective refractive index is $n_{\text{eff}_{\text{min}}} = -1.5$.

TiO₂ [39,40] and SrTiO₃ [69,70,72,73]. The two yield the same dielectric function $\epsilon_r(\omega)$ at the operating frequency. We also simulated a similar ADM but consisting of HPRs made of SrTiO₃ and found that it exhibits the same mode coupling effect (results not shown herein). The effective index reaches values as low as $n_{\text{eff}_{\text{min}}} = -7$, meaning that the effect of the mode coupling is stronger when a higher permittivity material is used ($\epsilon_r \simeq 300$ [70] instead of $\epsilon_r = 94$), because this heightens the resonances.

However, losses (imaginary part of $\epsilon_r(\omega)$) resulting from the TO₁ phonon greatly increase and therefore limits the operating range at terahertz frequencies. Besides, the real part of the dielectric function $\epsilon_r(\omega)$ falls down at higher frequency [70,72], which drastically modifies the Mie resonances. The lower permittivity of TiO₂ leads to greater side lengths a_m and a_e of each resonator (see equation 2) and therefore, it facilitates their fabrication. Consequently, TiO₂ is more suitable for ADM applications at THz frequencies.

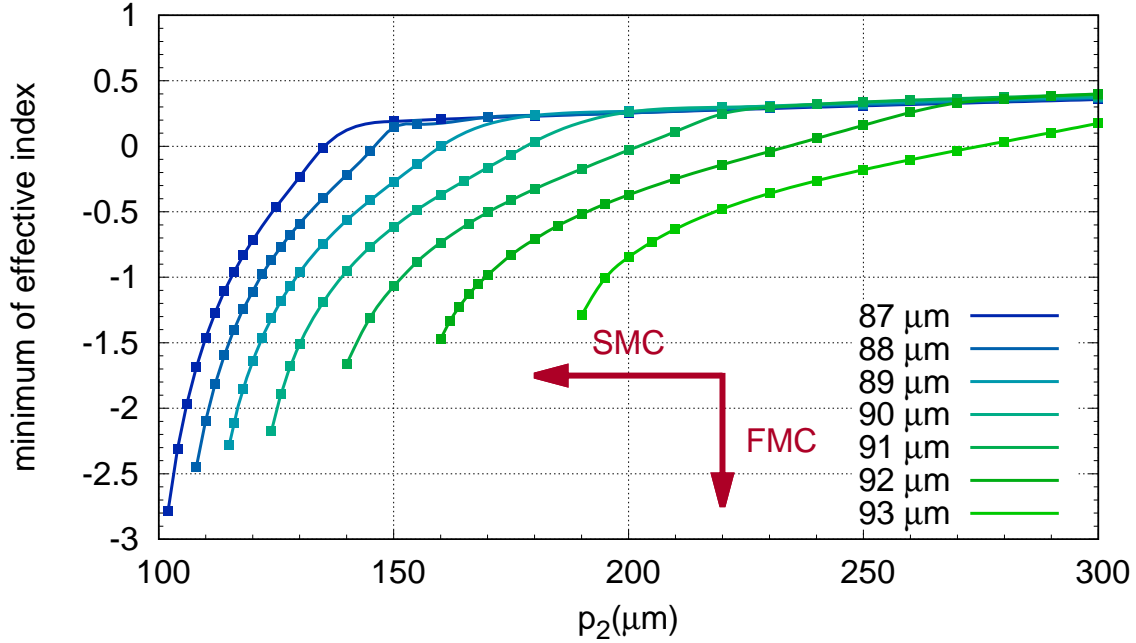


Figure 10. Effect of both mode couplings (*spatial* mode coupling (SMC) and frequency mode coupling (FMC)): minimal value of the effective refractive index n_{eff} in function of the distance p_2 between two resonators for several values of the side length a_e of the *electric* resonator. The side length of the *magnetic* resonator is $a_m = 60 \mu\text{m}$. The two arrows denote increasing mode coupling. The minimum of the effective index is $n_{eff_{min}} = -2.8$.

4. Conclusion

We have studied mode coupling effects in ADMs at terahertz frequencies and we show that the mode coupling has to be sufficiently strong to ensure negative effective index of refraction. Tuning the first two modes of Mie resonances of an ADM by adjusting the mode coupling allows to set the effective index from a near-zero value to a negative value. We studied both spatial mode coupling and frequency mode coupling. Increasing both brings the modes closer until they are merged. Thus, we highlight the frequency degeneracy of the first two resonance modes, namely, the two frequencies are equal, and the effective index is then undetermined. At the crossing point, the effective index reaches its lowest value.

5. Author contributions

É.A. supervised the study, analyzed the results and wrote the paper. S.M. made the simulation and analyzed the results.

Acknowledgments

The authors thank Aloyse Degiron for helpful discussion. É.A. thanks Fabrice Rossignol and Jean-Pierre Ganne for their help. This work has been funded by the Agence Nationale de la Recherche *TéraMétaDiel* project (number ANR-12-BS03-0009)

- [1] Popa B I and Cummer S A 2008 *Phys. Rev. Lett.* **100**(20) 207401 URL <http://link.aps.org/doi/10.1103/PhysRevLett.100.207401>
- [2] Richtmyer R D 1939 *Journal of Applied Physics* **10** 391–398 URL <http://scitation.aip.org/content/aip/journal/jap/10/6/10.1063/1.1707320>
- [3] O'Brien S and Pendry J B 2002 *Journal of Physics: Condensed Matter* **14** 4035
- [4] Pendry J B and Smith D R 2004 *Physics Today* **57** 37–43
- [5] Padilla W J, Basov D N and Smith D R 2006 *Materials Today* **9** 28 – 35 ISSN 1369-7021 URL <http://www.sciencedirect.com/science/article/pii/S1369702106715735>
- [6] Smith D R, Padilla W J, Vier D C, Nemat-Nasser S C and Schultz S 2000 *Phys. Rev. Lett.* **84**(18) 4184–4187 URL <http://link.aps.org/doi/10.1103/PhysRevLett.84.4184>
- [7] Ziolkowski R W 2003 *IEEE Transactions on Antennas and Propagation* **51** 1516–1529 ISSN 0018-926X
- [8] Engheta N and Ziolkowski R W 2005 *IEEE Transactions on Microwave Theory and Techniques* **53** 1535–1556 ISSN 0018-9480
- [9] Liu R, Degiron A, Mock J J and Smith D R 2007 *Applied Physics Letters* **90** 263504 URL <http://scitation.aip.org/content/aip/journal/apl/90/26/10.1063/1.2752120>
- [10] Ahmadi A and Mosallaei H 2008 *Phys. Rev. B* **77**(4) 045104 URL <http://link.aps.org/doi/10.1103/PhysRevB.77.045104>
- [11] Zhao Q, Zhou J, Zhang F and Lippens D 2009 *Materials Today* **12** 60 – 69 ISSN 1369-7021 URL <http://www.sciencedirect.com/science/article/pii/S1369702109703189>
- [12] Liu N, Liu H, Zhu S and Giessen H 2009 *Nature Photonics* **3** 157–162
- [13] Jahani S and Jacob Z 2016 *Nat Nano* **11** 23–36 URL <http://dx.doi.org/10.1038/nnano.2015.304>
- [14] Moitra P, Slovick B A, li W, Kravchenko I I, Briggs D P, Krishnamurthy S and Valentine J 2015 *ACS Photonics* **2** 692–698 URL <http://dx.doi.org/10.1021/acsp Photonics.5b00148>
- [15] Liu X, Zhao Q, Lan C and Zhou J 2013 *Applied Physics Letters* **103** 031910
- [16] Liu X, Bi K, Li B, Zhao Q and Zhou J 2016 *Opt. Express* **24** 20454–20460 URL <http://www.opticsexpress.org/abstract.cfm?URI=oe-24-18-20454>
- [17] Moitra P, Yang Y, Anderson Z, Kravchenko I I, Briggs D P and Valentine J 2013 *Nat Photon* **7** 791–795
- [18] Liu S, Sinclair M B, Mahony T S, Jun Y C, Campione S, Ginn J, Bender D A, Wendt J R, Ihlefeld J F, Clem P G, Wright J B and Brener I 2014 *Optica* **1** 250–256 URL <http://www.osapublishing.org/optica/abstract.cfm?URI=optica-1-4-250>
- [19] Luk'yanchuk B, Zheludev N I, Maier S A, Halas N J, Nordlander P, Giessen H and Chong C T 2010 *Nat Mater* **9** 707–715
- [20] Lepetit T, Akmansoy E, Ganne J P and Lourtioz J M 2010 *Phys. Rev. B* **82**(19) 195307 URL <http://link.aps.org/doi/10.1103/PhysRevB.82.195307>
- [21] Zhao Q, Kang L, Du B, Zhao H, Xie Q, Huang X, Li B, Zhou J and Li L 2008 *Phys. Rev. Lett.* **101**(2) 027402 URL <http://link.aps.org/doi/10.1103/PhysRevLett.101.027402>
- [22] Lepetit T, Akmansoy E, Pate M and Ganne J P 2008 *Electronics Letters* **44** 1119–1120 ISSN 0013-5194
- [23] Vendik I, Odit M and Kozlov D 2009 *Metamaterials* **3** 140 – 147
- [24] Kim J and Gopinath A 2007 *Phys. Rev. B* **76**(11) 115126 URL <http://link.aps.org/doi/10.1103/PhysRevB.76.115126>
- [25] Lepetit T, Akmansoy É and Ganne J P 2009 *Applied Physics Letters* **95** 121101 URL <http://scitation.aip.org/content/aip/journal/apl/95/12/10.1063/1.3232222>
- [26] Nemeč H, Kuzel P, Kadlec F, Kadlec C, Yahiaoui R and Mounaix P 2009 *Physical Review B (Condensed Matter and Materials Physics)* **79** 241108
- [27] Wheeler M S, Aitchison J S, Chen J I L, Ozin G A and Mojahedi M 2009 *Phys. Rev. B* **79** 073103
- [28] Ginn J C, Brener I, Peters D W, Wendt J R, Stevens J O, Hines P F, Basilio L I, Warne L K, Ihlefeld J F, Clem P G and Sinclair M B 2012 *Phys. Rev. Lett.* **108**(9) 097402 URL

- <http://link.aps.org/doi/10.1103/PhysRevLett.108.097402>
- [29] Schuller J A, Zia R, Taubner T and Brongersma M L 2007 *Phys. Rev. Lett.* **99**(10) 107401 URL <http://link.aps.org/doi/10.1103/PhysRevLett.99.107401>
- [30] Shi L, Tuzer T U, Fenollosa R and Meseguer F 2012 *Advanced Materials* **24** 5934–5938 ISSN 1521-4095 URL <http://dx.doi.org/10.1002/adma.201201987>
- [31] Zheludev N I and Kivshar Y S 2012 *Nat Mater* **11** 917–924
- [32] Gauffillet F, Marcellin S and Akmansoy E 2017 *IEEE Journal of Selected Topics in Quantum Electronics* **23** 1–5 ISSN 1077-260X
- [33] Liu N and Giessen H 2010 *Angewandte Chemie International Edition* **49** 9838–9852 ISSN 1521-3773 URL <http://dx.doi.org/10.1002/anie.200906211>
- [34] Zhang F, Kang L, Zhao Q, Zhou J and Lippens D 2012 *New Journal of Physics* **14** 033031 URL <http://stacks.iop.org/1367-2630/14/i=3/a=033031>
- [35] Zhang F, Sadaune V, Kang L, Zhao Q, Zhou J and Lippens D 2012 *Progress In Electromagnetics Research-Pier* **132** 587–601
- [36] Lannebère S, Campione S, Aradian A, Albani M and Capolino F 2014 *J. Opt. Soc. Am. B* **31** 1078–1086 URL <http://josab.osa.org/abstract.cfm?URI=josab-31-5-1078>
- [37] Marcellin S and Akmansoy E 2015 Negative index and mode coupling in all-dielectric metamaterials at terahertz frequencies *2015 9th International Congress on Advanced Electromagnetic Materials in Microwaves and Optics (METAMATERIALS)* pp 4–6
- [38] Lepetit T, Akmansoy E and Ganne J P 2011 *Journal of Applied Physics* **109** 023115
- [39] Matsumoto N, Hosokura T, Kageyama K, Takagi H, Sakabe Y and Hangyo M 2008 *Japanese Journal of Applied Physics* **47** 7725 URL <http://stacks.iop.org/1347-4065/47/i=9S/a=7725>
- [40] Berdel K, Rivas J, Bolivar P, de Maagt P and Kurz H 2005 *IEEE Transactions On Microwave Theory And Techniques* **53** 1266–1271
- [41] Depine R A and Lakhtakia A 2004 *Microw. Opt. Techn. Lett.* **41** 315–316
- [42] Cohn S B 1968 *IEEE Transactions on Microwave Theory and Techniques* **16** 218–227 ISSN 0018-9480
- [43] Kajfez D and Guillon P 1986 *Dielectric resonators* (Artech house)
- [44] Sethares J and Naumann S 1966 *IEEE Transactions On Microwave Theory And Techniques* **MT14** 2–& ISSN 0018-9480
- [45] Chen X, Grzegorzczak T M, Wu B I, Pacheco J and Kong J A 2004 *Phys. Rev. E* **70**(1) 016608 URL <http://link.aps.org/doi/10.1103/PhysRevE.70.016608>
- [46] Prodan E, Radloff C, Halas N J and Nordlander P 2003 *Science* **302** 419–422 ISSN 0036-8075 (*Preprint* <http://science.sciencemag.org/content/302/5644/419.full.pdf>) URL <http://science.sciencemag.org/content/302/5644/419>
- [47] Guo H, Liu N, Fu L, Meyrath T P, Zentgraf T, Schweizer H and Giessen H 2007 *Opt. Express* **15** 12095–12101 URL <http://www.opticsexpress.org/abstract.cfm?URI=oe-15-19-12095>
- [48] Abdeddaim R, Ourir A and de Rosny J 2011 *Phys. Rev. B* **83**(3) 033101 URL <http://link.aps.org/doi/10.1103/PhysRevB.83.033101>
- [49] Shen N H, Zhang L, Koschny T, Dastmalchi B, Kafesaki M and Soukoulis C M 2012 *Applied Physics Letters* **101** URL <http://scitation.aip.org/content/aip/journal/apl/101/8/1.1063/1.4748361>
- [50] Liu N, Guo H, Fu L, Kaiser S, Schweizer H and Giessen H 2007 *Advanced Materials* **19** 3628–3632 ISSN 1521-4095 URL <http://dx.doi.org/10.1002/adma.200700123>
- [51] Christ A, Martin O J F, Ekinici Y, Gippius N A and Tikhodeev S G 2008 *Nano Letters* **8** 2171–2175 PMID: 18578551 URL <http://dx.doi.org/10.1021/nl0805559>
- [52] Kanté B, Park Y S, O’Brien K, Shuldman D, Lanzillotti-Kimura N D, Jing Wong Z, Yin X and Zhang X 2012 *Nat Commun* **3** 1180
- [53] Nordlander P, Oubre C, Prodan E, Li K and Stockman M I 2004 *Nano Letters* **4** 899–903
- [54] van de Groep J, Coenen T, Mann S A and Polman A 2016 *Optica* **3** 93–99 URL <http://>

- [//www.osapublishing.org/optica/abstract.cfm?URI=optica-3-1-93](http://www.osapublishing.org/optica/abstract.cfm?URI=optica-3-1-93)
- [55] Nicolson A M and Ross G F 1970 *IEEE Trans. Instrum. Meas.* **19** 377–382
 - [56] Weir W 1974 *Proc. IEEE* **62** 33–36
 - [57] Szabo Z, Park G H, Hedge R and Li E P 2010 *IEEE Transactions on Microwave Theory and Techniques* **58** 2646–2653 ISSN 0018-9480
 - [58] Varadan V and Ro R 2007 *Microwave Theory and Techniques, IEEE Transactions on* **55** 2224–2230 ISSN 0018-9480
 - [59] Smith D R, Schultz S, Markoš P and Soukoulis C M 2002 *Phys. Rev. B* **65**(19) 195104 URL <http://link.aps.org/doi/10.1103/PhysRevB.65.195104>
 - [60] Koschny T, Markoš P, Smith D R and Soukoulis C M 2003 *Phys. Rev. E* **68**(6) 065602 URL <http://link.aps.org/doi/10.1103/PhysRevE.68.065602>
 - [61] Smith D R, Vier D C, Koschny T and Soukoulis C M 2005 *Phys. Rev. E* **71**(3) 036617 URL <http://link.aps.org/doi/10.1103/PhysRevE.71.036617>
 - [62] Alù A 2011 *Phys. Rev. B* **83**(8) 081102 URL <http://link.aps.org/doi/10.1103/PhysRevB.83.081102>
 - [63] Simovski C R 2011 *Journal of Optics* **13** 013001 URL <http://stacks.iop.org/2040-8986/13/i=1/a=013001>
 - [64] Ziolkowski R W 2004 *Phys. Rev. E* **70**(4) 046608 URL <http://link.aps.org/doi/10.1103/PhysRevE.70.046608>
 - [65] Alù A, Silveirinha M G, Salandrino A and Engheta N 2007 *Phys. Rev. B* **75**(15) 155410 URL <http://link.aps.org/doi/10.1103/PhysRevB.75.155410>
 - [66] Sihvola A 2005 *Progress In Electromagnetics Research-Pier* **51** 65–82 ISSN 1559-8985
 - [67] Spitzer W G, Miller R C, Kleinman D A and Howarth L E 1962 *Phys. Rev.* **126**(5) 1710–1721 URL <http://link.aps.org/doi/10.1103/PhysRev.126.1710>
 - [68] Barker A S 1966 *Phys. Rev.* **145**(2) 391–399 URL <http://link.aps.org/doi/10.1103/PhysRev.145.391>
 - [69] Han J, Wan F, Zhu Z and Zhang W 2007 *Applied Physics Letters* **90** –
 - [70] Matsumoto N, Fujii T, Kageyama K, Takagi H, Nagashima T and Hangyo M 2009 *Japanese Journal of Applied Physics* **48** 09KC11 URL <http://stacks.iop.org/1347-4065/48/i=9S1/a=09KC11>
 - [71] Gervais F m c and Piriou B 1974 *Phys. Rev. B* **10**(4) 1642–1654 URL <http://link.aps.org/doi/10.1103/PhysRevB.10.1642>
 - [72] Tsurumi T, Li J, Hoshina T, Kakemoto H, Nakada M and Akedo J 2007 *Applied Physics Letters* **91** 182905 URL <http://scitation.aip.org/content/aip/journal/apl/91/18/10.1063/1.2804570>
 - [73] Petzelt J, Ostapchuk T, Gregora I, Rychetský I, Hoffmann-Eifert S, Pronin A V, Yuzyuk Y, Gorshunov B P, Kamba S, Bovtun V, Pokorný J, Savinov M, Porokhonskyy V, Rafaja D, Vaněk P, Almeida A, Chaves M R, Volkov A A, Dressel M and Waser R 2001 *Phys. Rev. B* **64**(18) 184111 URL <http://link.aps.org/doi/10.1103/PhysRevB.64.184111>